Electronic Supporting Information

Engineering Fluorescence Intensity and Electron Concentration of Monolayer MoS$_2$ by Forming Heterostructures with Semiconductor Dots

Qiushi Feng,[1] Jia Shi,[2] Weiqiang Yang,[1] Weiheng Zhong,[1] Yuanzheng Li,[1] Heyu Chen,[1] Weizhen Liu,[1,3,]* Haiyang Xu,[1,]* Xinfeng Liu[2] and Yichun Liu[1]

[1]Centre for Advanced Optoelectronic Functional Materials Research and Key Laboratory of UV-Emitting Materials and Technology (Northeast Normal University), Ministry of Education, Changchun 130024, China

[2]Division of Nanophotonics, CAS Key Laboratory of Standardization and Measurement for Nanotechnology, CAS Center for Excellence in Nanoscience, National Center for Nanoscience and Technology, Beijing 100190, China

[3]National Demonstration Center for Experimental Physics Education (Northeast Normal University), Changchun 130024, China

*Email: wzliu@nenu.edu.cn and hyxu@nenu.edu.cn

Note 1 Mass-action-model

The mass-action-model correlated with the charged trion is applied to calculate the net electron concentration N_e of 1L-MoS$_2$, which is employed to estimate the doping level. Firstly, the populations of A exciton N_A and charged trion N_A^- from steady-states equation can be expressed as[1-3]:

$$N_A(n) = \frac{G}{\Gamma_{ex} + k_{tr}(n)} \qquad (S1)$$

$$N_A^-(n) = \frac{k_{tr}(n)}{\Gamma_{tr}} \cdot \frac{G}{\Gamma_{ex} + k_{tr}(n)} \qquad (S2)$$

where n represents the number of doping times, G stands for the optical generation rate of A exciton, $k_{tr}(n)$ is the formation rate of the charged trion from A exciton, Γ_{ex} and Γ_{tr} express the decay rate of A exciton and charged trion respectively. Secondly, the PL intensity proportional to the populations of the A exciton (charged trion) can be obtained as follows:

$$I_A(n) = \frac{AG\,\gamma_{ex}}{\Gamma_{ex} + k_{tr}(n)} \qquad (S3)$$

$$I_A^-(n) = \frac{k_{tr}(n)}{\Gamma_{tr}} \cdot \frac{AG\gamma_{tr}}{\Gamma_{ex} + k_{tr}(n)} \qquad (S4)$$

where coefficient A reprensents the collection efficiency of luminescence, γ_{ex} and γ_{tr} express the radiative recombination rate of the A exciton and charged trion respectively. According to previous reports, $\Gamma_{ex} = 0.002 \text{ps}^{-1}$, $\Gamma_{tr} = 0.02 \text{ps}^{-1}$ and $k_{tr}(0) = 0.5 \text{ ps}^{-1}$.[4-6] The

fitting parameters $AG\gamma_{ex}/AG\gamma_{tr}$ is 0.15[1]. Due to the $k_{tr} \gg \Gamma_i$ (i = ex, tr), the PL intensity can be approximately expressed as:

$$I_X(n) \approx \frac{AG\gamma_{ex}}{k_{tr}(n)} \quad (S5)$$

$$I_A^-(n) = \frac{AG\gamma_{tr}}{\Gamma_{tr}} \quad (S6)$$

Thirdly, based on the above equations, the corresponding relation correlated with the net electron concentration N_e of 1L-MoS$_2$ is shown below[7]:

$$\frac{N_A N_e}{N_A^-} = (\frac{16\pi m_A m_e}{h^2 N_A^-}) k_B T \exp(-\frac{E_b}{k_B T}) \quad (S7)$$

where k_B is the Boltzman constant, T is the temperature, E_b is the binding energy of charged trion near the band gap (~40 meV). The $m_e(0.35 m_0)$, $m_A(0.8 m_0)$ and $m_A^-(1.15 m_0)$ represent the effective mass of electrons, an exciton and a charged trion respectively, where m_0 is the mass of a free electron.[8] Finally, using these parameters, the spectral weight of I_A^-/I_{total} ($I_{total} = I_A + I_A^-$) can be presented as:

$$\frac{I_A^-}{I_{total}} = \frac{\frac{\gamma_{tr}}{\gamma_{ex}} \cdot \frac{N_A^-}{N_A}}{1 + \frac{\gamma_{tr}}{\gamma_{ex}} \cdot \frac{N_A^-}{N_A}} \approx \frac{4 \times 10^{-14} N_e}{1 + 4 \times 10^{-14} N_e} \quad (S8)$$

namely

$$N_e = \frac{x}{4(1-x)} \times 10^{14}, x = \frac{I_A^-}{I_{total}} \quad (S9)$$

Note 2 Preparation details of CVD-grown 1L-MoS$_2$ flakes

The synthesis of 1L-MoS$_2$ flakes by chemical vapor deposition (CVD) was carried out in a horizontal quartz tube furnace. As reaction sources, sulfur powder (Sigma-Aldrich, 99.99%, 500 mg) and molybdenum trioxide (MoO$_3$) powder (Sigma-Aldrich, 99.98%, 5 mg) were placed in two separate quartz boats. The sulfur powder was placed upstream at a distance of 31 cm from the MoO$_3$ powder which was put in the center of the tube furnace. Herein, a relatively high dosage of sulfur powder is used to ensure the full sulfurization of MoO$_3$, which is beneficial to reduce the sulfur vacancies and improve the crystallinity of prepared samples. Afterwards, SiO$_2$/Si substrates were placed downstream of the MoO$_3$ powder with a separation of 2 cm. Before heating, the quartz tube was purged with ultrapure N$_2$ gas to exhaust any remnant air. And then, the furnace was rapidly heated at a ramping rate of 15 °C/min to the preset temperatures (180 °C for the sulfur powder and 800 °C for the MoO$_3$ powder respectively, in consideration of the simultaneous evaporation of these two precursors) under a constant flow rate of 50 sccm of N$_2$ gas. The reaction took place at atmospheric pressure for 20 min during which the temperatures were held on. After that, the CVD system was naturally cooled down to room temperature under the protection of N$_2$ gas.

**Note 3 Preparation of carbon-dot aqueous solution**

Firstly, mixed powders of citric acid (0.961 g) and 3,4-diaminobenzoic acid (0.760 g), with the molar ratio of 1:1, were put into a 10 mL deionized water for stirring and dissolution. Then, the prepared mixed solution was sealed into a reaction kettle, and put into a baking oven for 5-hour reaction at 180 ^{o}C. Thirdly, the above reaction solution cooled down to room temperature naturally and experienced a dialysis processing with 950 mL deionized water for 24 hours. Finally, the dialyzed solution was put into a rotary evaporator for 3 hours evaporation, and a resultant carbon-dot aqueous solution with volume of ~30 mL and concentration of ~20 mg/L was obtained.

Figure S1
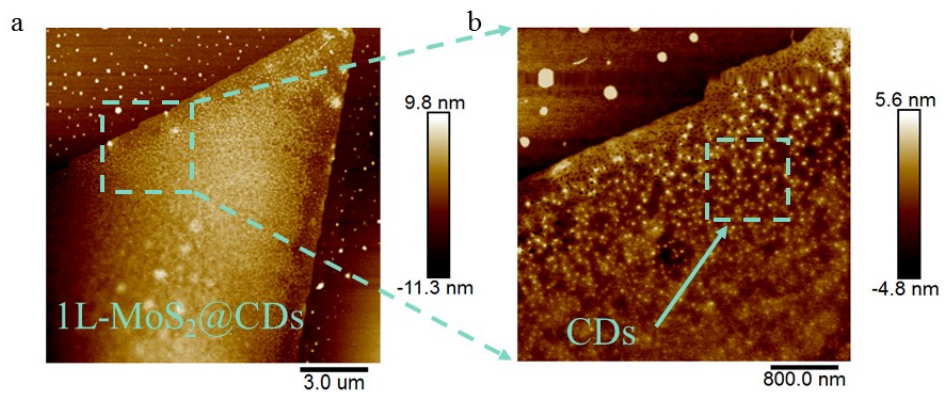
A typical AFM image of the 1L-MoS$_2$@CDs heterostructure. (b) Enlarged view of the cyan-dashed rectangular region in (a) for clarity; the white dots observed on the MoS$_2$ flake are the spin-coated CDs.

Figure S2
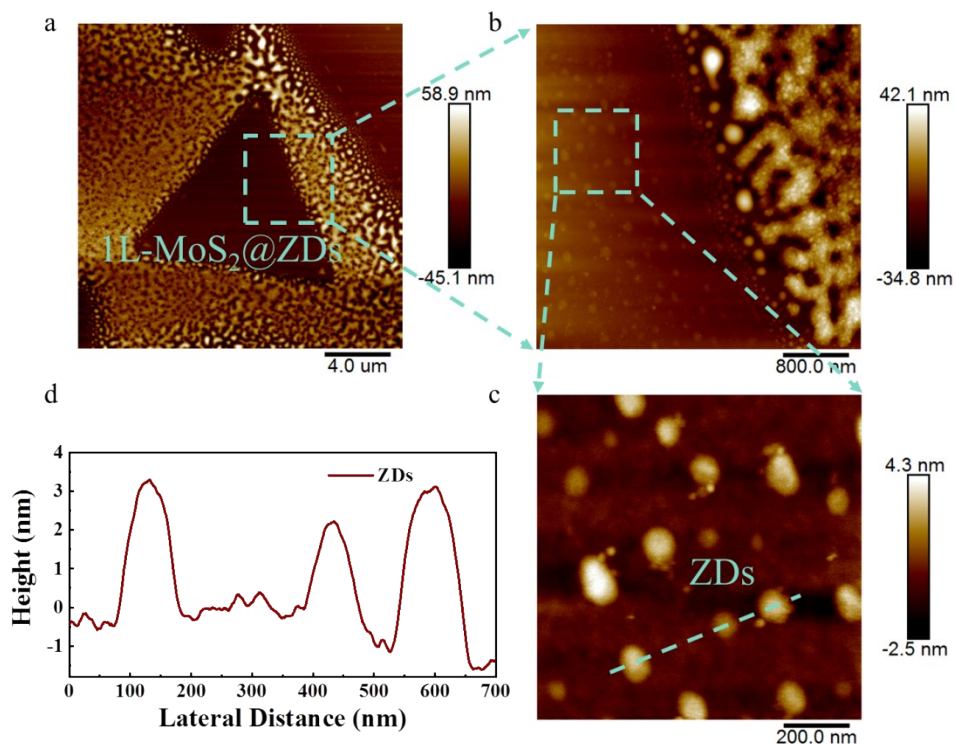
(a) An overall-view AFM image of the 1L-MoS$_2$@ZDs heterostructure; whitish region surrounding the 1L-MoS$_2$ triangular flake is the ZnO film depositing on the SiO$_2$/Si substrate. (b) Enlarged view of the cyan-dashed rectangular region in (a) with some faintly visible ZnO dots. (c) Enlarged view of the cyan-dashed rectangular region in (b) for clarity; the bright dots observed are ZnO-dots synthesized by ALD method. (d) AFM height scan of the prepared ZDs on 1L-MoS$_2$ flake (along the cyan dashed line in (c)), revealing the vertical height of these ZDs is about 3 to 4 nm.
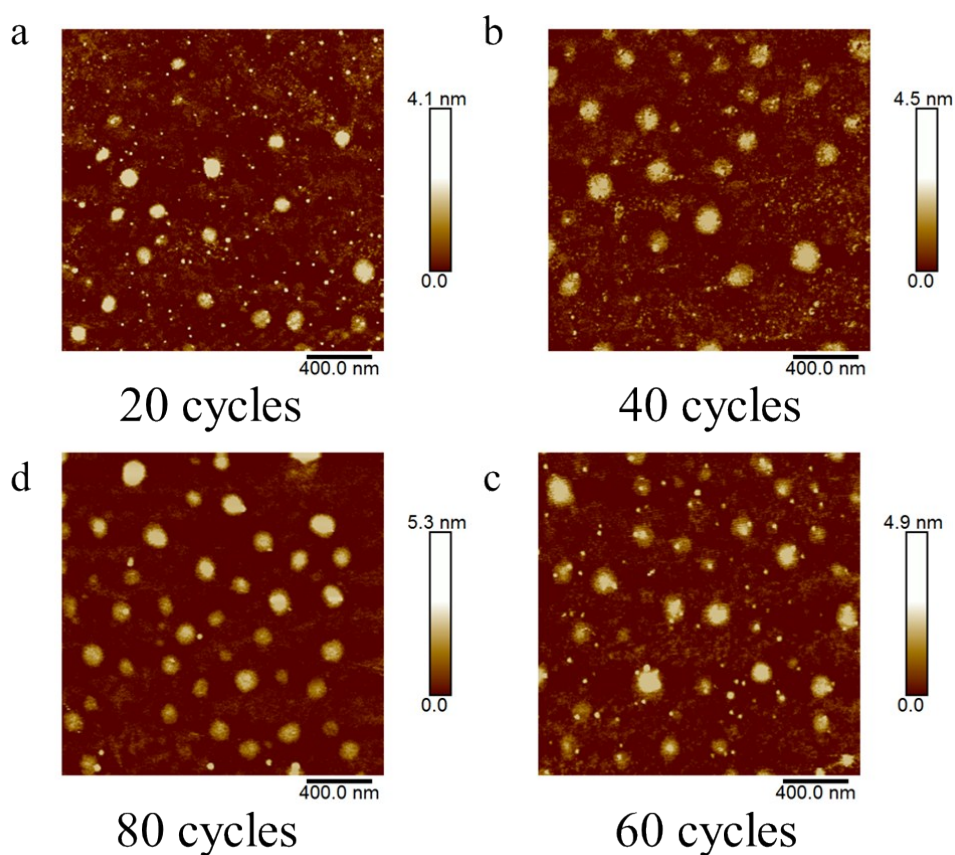
Figure S3

a 20 cycles
b 40 cycles
d 80 cycles
c 60 cycles

Table S1

Growth Cycle	Number of ZDs	Surface Coverage
0	0	0
20	18	0.09
40	20	0.15
60	24	0.18
80	41	0.26

ZnO dots with different ALD growth cycles from 20 to 80 are prepared in Figure S3 (a) to (d). The increased ALD growth cycle elevates the number density and surface coverage of ZDs on 1L-MoS$_2$ flakes, which will significantly change the fluorescence emission of 1L-MoS$_2$. This point has been discussed in detail in the main text.

Figure S4
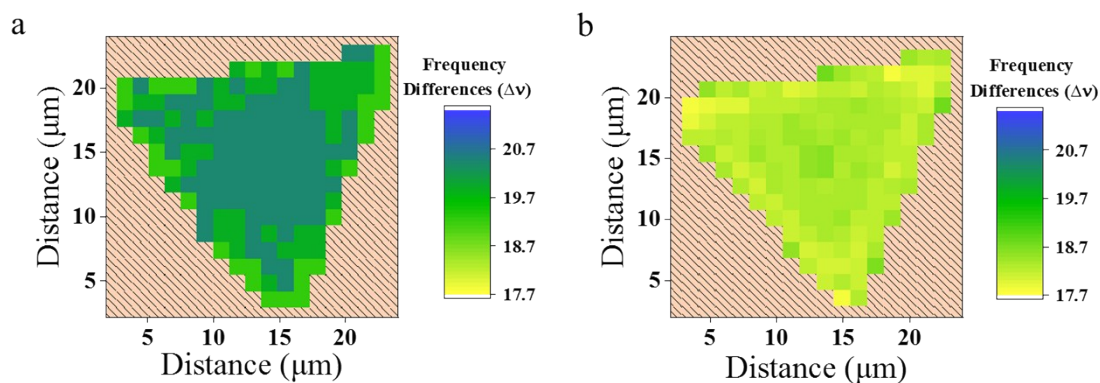
Raman Δv mappings of the obtained 1L-MoS$_2$ flake prior to (a) and after the spin-coating of CDs (b).

As can be seen from the **Fig.S4 (a)**, all measured Δv (frequency difference between the E_{2g}^1 and A$_{1g}$ modes) fall in the range of 19.2 to 20.5 cm^{-1}, confirming that the synthesized sample is uniform monolayer MoS$_2$. However, a noticeable and uniform redshift (approximately 1 cm^{-1}) compared with **Fig.S4 (b)**, is observed for the Δv mapping of 1L-MoS$_2$@CDs heterostructure in the **Fig.S4 (b)**. The above uniform redshift of Δv across the entire flake strongly illustrates that the n-doping of 1L-MoS$_2$ due to the coated CDs is homogeneous.

Figure S5
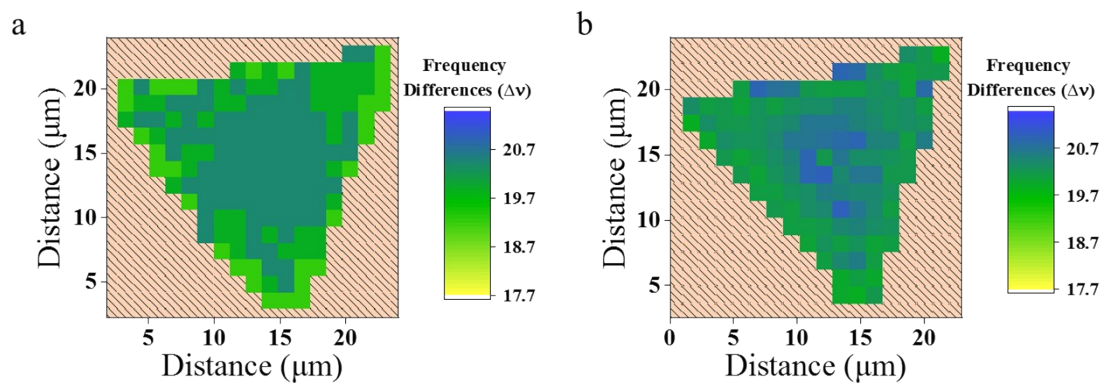
Raman Δv mappings of the obtained 1L-MoS$_2$ flake prior to (a) and after (b) the deposition of ZDs.

By carefully comparing the two pictures, it could be found that the Δv of the entire flake becomes larger, namely blueshift (approximately 0.5 cm^{-1}), after the deposition of ZDs, indicating that the p-doping modulation induced by these ZDs is uniform across the whole 1L-MoS$_2$. The observed Δv blueshift in **Figure 5** is a credible phenomenon, not just an unreliable conclusion drawn from a single point measurement.

Figure S6

| bare 1L-MoS$_2$ | 1L-MoS$_2$@CDs | 1L-MoS$_2$@ZDs |
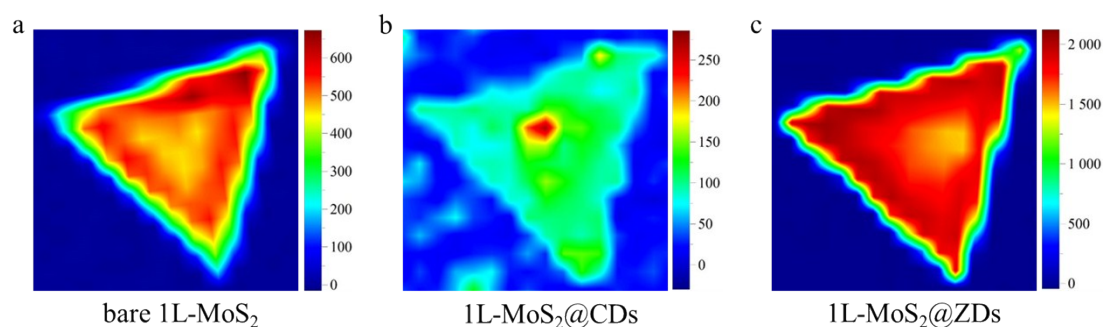
PL mappings of the obtained 1L-MoS$_2$ flake prior to (a) and after the spin-coating of CDs (b) and after the deposition of ZDs (c). It is noted that a relatively strong fluorescence emission is observed in the central block of 1b, which could be attributed to the PL from excessive fluorescent CDs gathering.

The PL measurement results in this paper were mainly collected from the center of the flakes. We also performed the PL mapping prior to and after the formation of heterostructures and observed uniform distribution of PL intensities across the whole MoS$_2$ flakes (see **Fig.S6**). Compared with bare 1L-MoS$_2$, the PL intensity of 1L-MoS$_2$@CDs is evenly quenched due to the uniform n-type doping to MoS$_2$ from CDs, whereas that of 1L-MoS$_2$@ZDs is homogeneously enhanced on account of the uniform p-type doping to MoS$_2$ from ZDs. The above measurement results prove that the fluorescence modulation of the semiconductor-dots to MoS$_2$ is uniformly distributed across the whole flake, rather than an unreliable conclusion just from some single points. Besides, we cannot ignore one interesting feature, namely the PL intensity of the edge region is weaker than that of the center region in all three pictures. The reason for this phenomenon is that there are dangling bonds existing in the edge region which are prone to introduce defect states.[9] Consequently, these defect states cause fluorescence quenching via non-radiative recombination channels.[10] On the contrary, there are fewer defect states and less impurities in the centre region, and thus the crystal lattice is relatively intact.[11] Therefore, PL spectra recorded from the flake centre region could more truly reflect the changes of charged trions and neutral excitons induced by

charge doping, avoiding the interference from defect states or impurity levels. So, in order to clearly demonstrate the influence of charge doping on the 1L-MoS$_2$ optical property, the spectra (including PL and Raman) given in the paper mainly come from the samples' central regions.

In fact, the trions/excitons may behave differently in the different zone of the MoS$_2$ flakes. In the central region, trions/excitons' behaviors are mainly affected by the charge doping due to the relatively perfect lattice alignment therein. However, there are defect states or dangling bonds in the edge or vertex angle regions, which can also modulate the PL behaviors of excitons and trions. Thus, the fluorescence tuning effect by charge doping may not be truly reflected in the flake edge regions.[9, 12] So, in order to clearly demonstrate the influence of charge doping on the 1L-MoS$_2$ optical property, the spectra (including PL and Raman) given in the paper mainly come from the samples' central regions.

Table S2

	A_1	$\tau_{1(ps)}$	A_2	$\tau_{2(ps)}$	$\tau_{eff(ps)}$
1L-MoS$_2$@CDs	1.50	53	0.059	2404	1557
bare 1L-MoS$_2$	1.23	57	0.033	1420	603
1L-MoS$_2$@ZDs	2.66	55	8.37	55	55

Fitting results of each parameter.

References

1.   S. Mouri, Y. Miyauchi and K. Matsuda, *Nano Lett.,* 2013, **13**, 5944.

2.   Z. W. Li, R. Q. Ye, R. Feng, Y. M. Kang, X. Zhu, J. M. Tour and Z. Y. Fang, *Adv. Mater.*, 2015, **27**, 5235.

3.   Y. Z. Li, X. S. Li, H. Y. Chen, J. Shi, Q. Y. Shang, S. Zhang, X. H. Qiu, Z. Liu, Q. Zhang, H. Y. Xu, W. Z. Liu, X. F. Liu and Y. C. Liu, *ACS Appl. Mater. Interfaces*, 2017, **9**, 27402.

4.   H. Y. Shi, R. S. Yan, S. Bertolazzi, J. Brivio, B. Gao, A. Kis, D. Jena, H. G. Xing and L. B. Huang, *ACS Nano*, 2013, **7**, 1072.

5.   K. F. Mak, K. L. He, C. G. Lee, G. H. Lee, J. Hone, T. F. Heinz and J. Shan, *Nat Mater.*, 2013, **12**, 207.

6.   Z. G. Nie, R. Long, L. F. Sun, C. C. Huang, J. Zhang, Q. H. Xiong, D. W. Hewak, Z. X. Shen, O. V. Prezhdo and Z. H. Loh, *ACS Nano*, 2014, **8**, 10931.

7.   H. Stolz and R. Zimmermann, *Phys. Stat. Sol.*, 2010, **94**, 135.

8.   T. Cheiwchanchamnangij and W. R. L. Lambrecht, *Phys Rev B*, 2012, **85**, 205302.

9.   D. Wu, X. Li, L. Luan, X. Y. Wu, W. Li, M. N. Yogeesh, R. Ghosh, Z. D. Chu, D. J. Akinwande, Q. Niu, K. J. Lai, *Proc. Natl. Acad. Sci. USA*, 2016,**113**,8583-8.

10.   A. Zafar, H. Y. Nan, Z. Zafar, Z. T. Wu, J. Jiang, Y. M. You, Z. H. Ni, *Nano Res.*, 2017,**10**,1608-17.

11.   W. T. Hsu, L. S. Lu, D. Wang, J. K. Huang, M. Y Li, T. R. Chang, Y. C. Chou, Z. Y Juang, H. T. Jeng, L. J. Li ,W. H. Chang, *Nat. Communn.*, 2017,**8**,2.

12.   D. L. C. Ky, B. C. T. Khac, C. T. Le, Y. S. Kim, K. H. Chung, *Friction*, 2018,**6**,395-406.